BIALLELIC MUTATIONS IN *SORD* CAUSE A COMMON AND POTENTIALLY TREATABLE HEREDITARY NEUROPATHY WITH IMPLICATIONS FOR DIABETES

Andrea Cortese[1,2,3,#,], Yi Zhu[4,5,#], Adriana Rebelo[1,#], Sara Negri[6], Steve Courel[1], Lisa Abreu[1], Chelsea J Bacon[7], Yunhong Bai[7], Dana M Bis-Brewer[1], Enrico Bugiardini[2], Elena Buglo[1], Matt C Danzi[1], Shawna ME Feely[7], Alkyoni A Fragkouli[2], Nourelhoda A Haridy[2,8], Inherited Neuropathy Consortium, Rosario Isasi[1], Alaa Khan[2], Matilde Laurà[2], Stefania Magri[9], Menelaos Pipis[2], Chiara Pisciotta[10], Eric Powell[1], Alexander M Rossor[2], Janet Sowden[11], Stefano Tozza[12], Jana Vandrovcova[2], Julia Dallman[13], Elena Grignani[6], Enrico Marchioni[14], Steven S Scherer[15], Beisha Tang[16], Zhiqiang Lin[17], Abdullah Al-Ajmi[18], Rebecca Schüle[19,20], Matthis Synofzik[19,20], Thierry Maisonobe[21], Tanya Stojkovic[22], Michaela Auer-Grumbach[23], Mohamed A Abdelhamed[8], Sherifa A. Hamed[8], Ruxu Zhang[17], Fiore Manganelli[12], Lucio Santoro[12], Paola Saveri[9], Franco Taroni[9], Davide Pareyson[10], Henry Houlden[2], David N Herrmann[11], Mary M Reilly[2], Michael E Shy[7], Grace Zhai[4,5], Stephan Zuchner[1]

[1] Dr. John T. Macdonald Foundation Department of Human Genetics and John P. Hussman Institute for Human Genomics, University of Miami Miller School of Medicine, Miami, Florida, USA.

[2] Department of Neuromuscular Disease, UCL Queen Square Institute of Neurology and The National Hospital for Neurology, London, UK

[3] Department of Brain and Behavioral Sciences, University of Pavia, Pavia, Italy.

[4] Department of Molecular and Cellular Pharmacology, University of Miami Miller School of Medicine, Miami, Florida, USA

[5] Program in Molecular and Cellular Pharmacology, University of Miami Miller School of Medicine, Miami, Florida, USA

[6] Environmental Research Center, Istituiti Clinici Scientifici Maugeri IRCCS, Pavia, Italy

[7] Department of Neurology, University of Iowa Carver College of Medicine, Iowa City, Iowa, USA

[8] Department of Neurology and Psychiatry, Faculty of Medicine, Assiut University Hospital, Assiut, Egypt

[9] Unit of Medical Genetics and Neurogenetics, Fondazione IRCCS Istituto Neurologico Carlo Besta, Milan, Italy

[10] Unit of Rare Neurodegenerative and Neurometabolic Diseases, Department of Clinical Neurosciences, Fondazione IRCCS Istituto Neurologico Carlo Besta, Milan, Italy

[11] Department of Neurology, University of Rochester, Rochester, NY, USA

[12] Department of Neuroscience, Reproductive Sciences and Odontostomatology, University of Naples "Federico II", Naples, Italy

[13] Department of Biology, University of Miami, Coral Gables, Florida, USA.

[14] IRCCS Mondino Foundation, Pavia, Italy

[15] Department of Neurology, Perelman School of Medicine, University of Pennsylvania, Philadelphia, Pennsylvania USA.

[16] National Clinical Research Center for Geriatric Disorders, Central South University, Changsha, 410078, Hunan Province, China

[17] Department of Neurology, The Third Xiangya Hospital, Central South University, Changsha, 410013, Hunan Province, China

[18] Division of Neurology, Department of Medicine, Al-Jahra Hospital, Kuwait

[19] Department of Neurodegenerative Disease, Hertie-Institute for Clinical Brain Research, and Center for Neurology, University of Tübingen, Tübingen, Germany

[20] German Center of Neurodegenerative Diseases (DZNE), Tübingen, Germany

[21] AP-HP, G-H Pitié Salpêtrière, Department of Neurophysiology, Paris France.

[22] G-H Pitié-Salpêtrière, Centre de Référence des Maladies Neuromusculaires, Paris Nord/Est/Ile de France, Paris, France.

[23] Department of Orthopaedics and Traumatology, Medical University of Vienna, Vienna, Austria

# Authors contributed equally

Correspondence

Andrea Cortese, MD, PhD
Andrea.cortese@ucl.ac.uk
Department of Neuromuscular Disease
UCL Queen Square Institute of Neurology
The National Hospital for Neurology
Queen Square
London
WC1N 3BG
United Kingdom

Stephan Zuchner, MD, PhD, FAAN
SZuchner@med.miami.edu
University of Miami Miller School of Medicine
Biomedical Research Building (BRB)
Room 616, LC: M-860
1501 NW 10th Avenue
Miami, FL 33136, USA

R. Grace Zhai, PhD
gzhai@med.miami.edu
University of Miami Miller School of Medicine
RMSB 6069, LC: R-189
1600 NW 10 AVE
Miami, FL 33136, USA

SUMMARY

Here we demonstrate biallelic mutations in *sorbitol dehydrogenase* (*SORD*) as the most frequent recessive form of hereditary neuropathies. We identified 45 cases from 38 families across multiple ethnicities, carrying a particular nonsense mutation in *SORD*, c.753delG; p.Ala253GlnfsTer27, either in homozygous or compound heterozygous state with a second variant. With an allele frequency of 0.004 in healthy controls, the p.Ala253GlnfsTer27 variant represents one of the most common pathogenic alleles in humans. SORD is an enzyme that converts sorbitol into fructose, in the two-step polyol pathway that has been implicated in diabetic neuropathy. In patient-derived fibroblasts, we find a complete loss of SORD protein as well as increased intracellular sorbitol. Also, serum fasting sorbitol level was over 100 times higher in patients homozygous for the p.Ala253GlnfsTer27 mutation compared to healthy individuals. In *Drosophila*, we show that loss of *SORD* orthologues causes synaptic degeneration and progressive motor impairment. Reducing the polyol influx by treatment with aldose reductase inhibitors normalized intracellular sorbitol levels in patient fibroblasts and in *Drosophila*, and also dramatically ameliorated motor and eye phenotypes. Together, these findings establish a potentially treatable cause in a significant fraction of patients with inherited neuropathies and may contribute to a better understanding of the pathophysiology of diabetic neuropathy.

INTRODUCTION

Hereditary neuropathies, also known as Charcot-Marie-Tooth disease (CMT), are clinically and genetically heterogenous conditions affecting the peripheral nerves. CMT is classified according to the motor conduction velocity in upper limb nerves as primarily demyelinating (CMT1) or axonal (CMT2). Distal hereditary motor neuropathy (dHMN) represents a form of CMT2 in which the burden of disease falls predominantly or exclusively on motor nerves (1). As opposed to CMT1, for which over 90% of cases have mutations in known genes, only 20 to 30% of CMT2 and dHMN patients receive a genetic diagnosis (2). Since up to 70% of CMT2 and dHMN cases are sporadic, identifying candidate pathogenic genes from single cases remains challenging also for next-generation sequencing techniques.

RESULTS

Identification of biallelic *SORD* mutations in undiagnosed inherited neuropathies

We took advantage of the largest collection of over 1,100 CMT patients in whom whole exome sequencing (WES) and/or whole genome sequencing (WGS) has been performed in the GENESIS analysis platform (genesis-app.com) (3). We specifically looked for genes for which significant DNA variants are present in multiple families as well as for individual alleles overrepresented in CMT cases. By querying a subset of 598 undiagnosed CMT patients for recessive nonsense variants in genes shared by > 3 families and with minor allele frequency in the gnomAD control database of <1%, we identified 12 cases from 11 unrelated families carrying a homozygous c.753delG; p.Ala253GlnfsTer27; chr15:45361217 (hg19, rs55901542) variant in *SORD* (NM_003104.6). Four more cases from three unrelated families carried the heterozygous p.Ala253GlnfsTer27 variant together with a second variant: c.298C>T; p.Arg100Ter in family 2, c.329G>C; p.Arg110Pro in family 3, and c.458C>A; p.Ala153Asp in II-1 and II-2 of family 14 (**Fig. 1A-D and Supplementary Fig. 1, Supplementary Table 2**). All variants, but p.Arg110Pro, represented loss-of-function (LOF) alleles. Interestingly, the p.Arg110Pro change is adjacent to the previously reported p.Tyr111Phe (corresponding to p.Tyr110Phe in rat), which was shown to abolish SORD enzymatic activity and destabilize the protein (4). Biallelic non-sense variants in *SORD* were absent from our internal disease controls (4590 WES on GENESIS platform from individuals affected by diverse neurological conditions but not CMT).

SORD has a non-functional highly homologous paralogue, the pseudogene *SORD2P*, which is thought to have arisen from the duplication of *SORD* within a 0.5 Mb region on chromosome 15 (5) (**Fig. 1E**). Notably, the c.753delG; p.Ala253GlnfsTer27 mutation in exon 7 of *SORD* is fixed in the pseudogene *SORD2P* in over 95% of control chromosomes, along with

numerous additional exonic indel mutations, which prevent effective translation of *SORD2P* (6,7). In order to specifically amplify *SORD*, but not *SORD2P,* in Sanger confirmation studies, we designed primers that took advantage of nucleotide sequence differences and distinct retrotransposon insertions in both genic regions (**Supplementary Table 1**). Because of the high similarity of the regions, a nested PCR approach was necessary to obtain specific amplification of exon 7 of *SORD* and distinguish it from the homologous region in *SORD2P.* We were able to confirm by Sanger sequencing the presence of the variants detected by WES or WGS in all cases and provide segregation data in immediate relative carriers (**Fig. 1F and Supplementary Fig. 1**).

We then screened an independent set of 103 unresolved CMT2/dHMN cases, for which WES had been performed at the UCL Institute of Neurology in London, UK, and identified nine cases from six unrelated families carrying the homozygous p.Ala253GlnfsTer27 mutation in *SORD* (8.7%). A third independent set of 297 recessive or sporadic CMT2/dHMN patients was screened by Sanger sequencing of exon 7 of *SORD*; this was extended to the other coding exons when the p.Ala253GlnfsTer27 allele was identified. This screening revealed 20 additional cases (7%) from 18 families with biallelic mutations in *SORD*: 16 cases with a homozygous p.Ala253GlnfsTer27 mutation and four cases with p.Ala253GlnfsTer27 in compound heterozygous state with a second likely pathogenic variant. The latter included a c.964G>A; p.Val322Ile allele in family 29, a 275bp deletion c.316_425+165del, Cys106Ter in exon 4 in family 30, a *de novo* c.28C>T; p.Leu10Phe change in family 32, and a c.895C>T; p.Arg299Ter variant in family 33; all had a minor allele frequency (MAF) of < 0.0001 in gnomAD (7). The residues affected by missense mutations are highly conserved across multiple species (**Fig. 1D**) with GERP scores greater than 3 (**Supplementary Table 2**). Further, biallelic non-sense variants in *SORD* were absent from 4,598 index cases affected by distinct neurological disorders other than CMT present in the GENESIS database.

The allelic carrier frequency of the p.Ala253GlnfsTer27 variant in the control population is 0.004 based on an allelic count of 623 out of 142,588 genomes on gnomAD v3 database (7), ranging from 0.002 in Africans and Asians to 0.005 in Europeans, 0.007 in Latinos and up to 0.03 in the Amish population. Also, there is only one East-Asian male individual on gnomAD v3 database is homozygote for the p.Ala253GlnfsTer27 variant in SORD. Of note, in the previous gnomAD exome set (GnomAD v2.1.1) the p.Ala253GlnfsTer27 change was detected at a significantly lower rate at MAF =0.00008, due to failure to pass random forest filters. GENESIS uses the FreeBayes software for exome variant calling (3), which may have resulted in an allele frequency ($MAF_{GENESIS}$ = 0.003; 27 alleles in 8,896 chromosomes) closer to the gnomAD v3 genome based call set.

We further performed Sanger sequencing of 600 healthy controls, including 300 samples of European, 100 samples of Turkish and 200 samples of Middle Eastern origin, and identified three heterozygous, but no homozygous, p.Ala253GlnfsTer27 alleles (MAF = 0.0025). As shown in **Supplementary Table 2**, we identified Ala253GlnfsTer27 in neuropathy patients of Caucasian, Asian, and African ancestry further rejecting the hypothesis of a historically recent founder mutation. In summary, these calculations support an estimated *SORD* neuropathy prevalence of ~1/100,000 individuals caused by homozygous p.Ala253GlnfsTer27 alleles alone, making this specific variant the most common individual pathogenic allele in biallelic state in inherited neuropathies (**Supplementary Table 3**) and one of the most common alleles for any recessive Mendelian disease (8,9).

Clinical features of patients with *SORD* neuropathy

Altogether, we identified 45 individuals from 38 unrelated families with biallelic mutations in *SORD* (**Table 1 and Supplementary Table 4**). Of note, 69% of cases were sporadic, with no evidence of family history or consanguinity, but were clinically diagnosed as having CMT based on the presence of a slowly progressive neuropathy, often accompanied by foot deformities. The formal clinical diagnosis was axonal CMT in 51% (N=23), distal HMN in 40% (N=18), and intermediate CMT in 9% (n=4) of cases. The mean age of onset of the neuropathy was 17 ± 8 years and difficulty walking was the most common complaint at onset. Delayed motor milestones were uncommon, but two thirds of the patients reported foot deformities, indicating that the neuropathy probably started earlier in life. All individuals had limb weakness, but only one-half had sensory impairment. Weakness was mild in distal upper limbs and ranged from mild to near complete paralysis in the distal lower limbs. Proximal muscles of the upper and lower limbs were typically unaffected. Seven patients had upper limb tremor, four had mild scoliosis and two had mild hearing loss. One case (case 14) had a concurrent and likely unrelated syndromic disorder encompassing dysmorphic features and static encephalopathy since the age of three years, and spastic ataxia with evidence of cerebellar atrophy on brain MRI. Another case (case 36), carrying a compound heterozygous p.Ala253GlnfsTer27/p.Val322Ile genotype, presented with earlier onset of the disease and severe neuropathy. The Val322Ile variant was not identified in any other patient of this study, is present in three subjects in gnomAD and has conflicting in silico predictions from tolerated to disease causing. None of the patients had cataracts nor involvement of other organs. Using the CMT neuropathy score (10) , after 17 ± 11 years of disease duration the neuropathy was mild in 67% (N=30), moderate in 31% (N=14), and severe in one case. Ankle-foot orthosis

during walking was used by 42% of patients (N=19); one patient required unilateral support and one patient was wheelchair-dependent. Detailed nerve conduction studies were available in 42 patients and invariably showed a motor axonal neuropathy, with intermediate reduction of conduction velocities in 26% (N=11, mean conduction velocity in upper limbs = 39±3 m/s, range 32-42 m/s) and decreased or absent amplitudes of sensory action potentials in 26% (N=11).

Loss of SORD enzymatic activity and increased serum fasting sorbitol level

SORD is a homotetramer of 38-kDa subunits and is widely expressed in mammalian tissues (4,11,12). It is the second enzyme of the two-step polyol pathway, in which aldose reductase converts glucose into sorbitol, a relatively nonmetabolizable sugar, which is then oxidized to fructose by SORD (**Fig. 2A**). To gather further insights into the functional consequences of recessive mutations in *SORD*, we next assessed SORD protein expression in fibroblasts from four independent healthy controls compared to four unrelated affected individuals with homozygous p.Ala253GlnfsTer27, one patient with compounded p.Ala253GlnfsTer27 / p.Arg299Ter variants, and two unaffected heterozygous carriers of p.Ala253GlnfsTer27. SORD protein was absent in all patients and the SORD levels were reduced in unaffected carriers compared to controls (**Fig. 2B**). Accordingly, intracellular sorbitol concentrations were over 10 times higher in patient fibroblasts compared to controls (**Fig. 2C**). We next tested the fasting sorbitol level in serum from ten patients carrying the homozygous p.Ala253GlnfsTer27 mutation and ten unrelated controls and found it was over 100 times higher (14.82 ± 0.780 vs 0.046 ± 0.004 mg/L, $p<0.0001$), confirming the lack of SORD enzymatic activity in patients.

***Drosophila melanogaster* model of *SORD* deficiency recapitulates the disease phenotype**

To further explore the pathophysiology of *SORD* mutations *in vivo*, we established *Drosophila melanogaster* models of *SORD* deficiency. *Drosophila* has two functional *Sord* proteinss - *Sodh1* (NP_001287203.1) and *Sodh2* (NP_524311.1) - that are 75% and 73% identical with human SORD protein (NP_003095.2), respectively, and 90% identical with each other (13). We obtained the $Sodh2^{MB01265}$ mutant allele of *Sodh2* in which a transposon disrupts the gene (14). Homozygous *Sodh2* ($Sodh2^{MB01265/MB01265}$) mutants are viable with normal life span (**Supplementary Fig. 2**), and, as described later, 10 days after eclosion (DAE) sorbitol level was significantly increased in the fly heads (**Fig. 4B**), consistent with our observations in patient fibroblasts. To determine whether $Sodh2^{MB01265/MB01265}$ mutants had a neurodegenerative phenotype, we examined the visual system, in which subtle neuronal and synaptic pathological changes can be detected (15). Axons of the outer photoreceptors traverse the lamina cortex and

make synaptic connections with lamina monopolar neurons (**Fig. 3A**). In the control (*yw*) flies at 2 DAE, the lamina cartridges of photoreceptor synapses can be visualized in the xy- and xz-planes, respectively (**Fig. 3B**). We observed a loss of photoreceptor terminals in the lamina layer of *Sodh2*$^{MB01265/MB01265}$ mutants at 2 days after eclosion (DAE) (**Fig. 3C**) - visualized as vacuole-like structures of reduced fluorescence after labeling with antibodies against neuronal membranes (horseradish peroxidase, HRP) and synaptic active zones (brunchpilot, BRP) (**Fig. 3C, D**). This phenotype was more severe at 10 DAE, with more numerous and larger vacuole-like structures distributed across the synaptic lamina layer (**Fig. 3C, D**). To validate our findings, we generated a second model by neuronal-specific knocking down of both Sodh1 and Sodh2, resulting in age-dependent vacuole-like structures formation **(Supplementary Fig. 3**) but normal life span (**Supplementary Fig. 2**), similar to that of the Sodh2$^{MB01265/MB01265}$ flies. We also found that the locomotor activities of both loss-of-function models were significantly worse than that of the control (yw) flies at a late-stage (40 DAE) (**Fig. 3E, F**), consistent with the progressive, age-dependent neuromuscular dysfunction seen in our patients. Taken together, *Drosophila* models of SORD deficiency recapitulate key phenotypes in the patients, including 1) a normal lifespan, 2) progressive and age-dependent synaptic degeneration and locomotor deficiency.

Treatment with aldose reductase inhibitors normalizes intracellular sorbitol and rescues the phenotype in *Drosophila melanogaster*

We investigated the possibility that SORD-associated hereditary neuropathy could be treated. Pharmacological inhibition of aldose reductase, the enzyme upstream of SORD, has been shown to reduce detrimental sorbitol accumulation in cellular and animal model of diabetes (16–20), and in humans (21–23). We thus tested the effect of two commercially available aldose reductase inhibitors (ARI), Epalrestat and Ranirestat, on intracellular sorbitol accumulation in patient fibroblasts lacking functional SORD. Patient and control fibroblasts were grown for 72 hrs in the presence or absence of Epalrestat (100 μM) or Ranirestat (10 μM) and intracellular sorbitol levels were measured thereafter. In patient fibroblasts both Epalrestat and Ranirestat significantly reduced sorbitol levels (**Fig. 4A**).

Next, we fed the *Drosophila* models of SORD deficiency with Epalrestat (80 μg/ml) and Ranirestat (80 μg/ml) or vehicle dymethyil sulfoxide (DMSO) starting at 2 DAE. At 10 DAE, the heads of DMSO-treated *Sodh2*$^{MB01265/MB01265}$ flies had significantly increased sorbitol but treatment with either Epalrestat or Ranirestat was able to reduce sorbitol levels to those observed in control (yw) flies (**Fig. 4B**), Epalrestat or Ranirestat rescued the locomotor activities of both *Sodh2*$^{MB01265/MB01265}$ flies and flies with neuronal specific knockdown of both *Sodh*1 and *Sodh2* to

the levels of control (*yw*) flies (**Fig. 4C, Supplementary Fig. 4**) and restored the age-dependent synaptic defects in *Sodh2*$^{MB01265/MB01265}$ mutant flies, by reducing the number of vacuole-like structures and restoring the localization of synaptic cytomatrix protein BRP at both 10 and 40 DAE (**Fig. 4D-G**). In contrast, the loss of synaptic termini was so advanced in DMSO/vehicle-treated flies at 40 DAE that neighboring vacuoles fused to form much larger vacuole-like structures that encompassed multiple synaptic cartridges (**Fig. 4D**).

DISCUSSION

Thus, recessive *SORD* mutations are a novel cause of inherited neuropathy. Genetic data from our cohort as well as from control databases suggest that the predominant pathogenic variant in *SORD*, c.753delG; p.Ala253GlnfsTer27, with a carrier frequency of ~3/1,000 individuals is the most common recessive cause of neuropathy identified to date and represents one of the most common specific alleles causing a recessive Mendelian disease. Indeed, with a frequency in undiagnosed CMT2 and dHMN cases of up to ~10%, the p.Ala253GlnfsTer27 variant will likely account for a significant portion of the diagnostic gap in inherited axonal neuropathies; rivaled only by the common dominant CMT2 gene *MFN2* (24). It is intriguing that, despite their frequency, mutations in *SORD* were not previously identified as a cause of CMT. We speculate that widely used next-generation sequencing analysis pipelines had difficulties to call variants in *SORD* in the presence of the homologous *SORD2P* pseudogene. Other known pathogenic variants have previously been shown to be concealed by the presence of pseudogenes (25). It is tempting to speculate that the appearance of the common c.753delG; p.Ala253GlnfsTer27 pathogenic allele could have arisen from interlocus gene conversion between SORD2P, where c.753delG is fixated in the absence of selective pressure, and SORD. Indeed, interlocus gene conversion is increasingly recognised as a mechanism causing human inherited disease (26–28). If this hypothesis was confirmed it would offer an intriguing mechanistic parallelism placing nonallelic homologous recombination, resulting in unequal crossover, as in PMP22 duplication/deletion causing CMT1A (29), and gene conversion of SORD, at the centre of the most common forms of demyelinating and axfonal CMT, respectively. However, no other nucleotide was changed in the nearby region of SORD to resemble SORD2P sequence. Therefore, a single-base deletions resulting from DNA replication errors along this homopolymeric repeats of G/C nucleotides, independently occurring in both SORD and SORD2P, could also represent an alternative and valid hypothesis.

The pathogenicity of *SORD* mutations is further supported by the *in vitro* data in patient-derived fibroblasts, which showed absent SORD protein and intracellular sorbitol accumulation,

and the dramatically higher fasting sorbitol level in patients' serum, which itself represents a promising biomarker for this condition. Two *in vivo Drosophila* models recapitulated key aspects of the human phenotype - increased sorbitol levels, as well as progressive synaptic degeneration and motor impairment. We propose enzymatic loss-of-function and subsequent sorbitol accumulation as the mechanism of action for SORD associated CMT. This conclusion is in accord with the finding that pharmacological inhibitors of SORD worsen neuropathy in diabetic rats (30,31).

Our findings do not fully elucidate yet the mechanism of axonal damage caused by SORD deficiency: one or more of the known effects of decreased SORD activity, including increased sorbitol level, cellular osmolarity, oxidative stress and decreased NADPH levels, are plausible (32,33). Mice that have significantly reduced levels of SORD protein due to an intronic splicing mutation (C57BL/LiA mice), bred and fed according to the standard laboratory conditions, do not develop neuropathy or even slowed nerve conduction velocities (34–36). This is possibly due to a difference in sugar metabolism between human and mouse since standard mouse chow consists of a low-sugar diet compared to humans (37) and flies, which are fed on a sugar-based diet. Indeed, SORD deficiency does aggravate the cataract and neuropathy in rodent models of diabetes (30,35,36). Based on patient clinical data and the late-onset phenotype observed in flies it will be important to examine ageing C57BL/LiA mice, or test the effect on the peripheral nerves of a higher sugar consumption, as well as create other models of SORD deficiency.

Our study further unravels a central role of the polyol pathway in peripheral nerve metabolism and survival in normoglycemic conditions. Although the mechanism by which increased intracellular sorbitol leads to selective degeneration of peripheral axons is yet unknown, the observation of increased sorbitol levels in patient derived cells in this study has promising implications, both as a biomarker of SORD-associated CMT and as a target for future therapeutic interventions, including methods for substrate reduction, gene replacement or correction, and SORD enzyme substitution. Accordingly, we have demonstrated in preclinical studies the beneficial effects of substrate reduction via ARI application in human derived cells and *Drosophila* models. Epalrestat is currently marketed in few countries for the treatment of diabetic complications (20) while Ranirestat has been advanced into late stages of clinical trials (22,23). Both drugs showed a good safety profile in patients with diabetic neuropathy. Whether those drugs may also represent a safe and effective approach for the treatment of SORD-associated inherited

neuropathy, given their known risk of off target effects and inducing more widespread metabolic alterations, will need to be addressed by future studies.

Finally, as an example of rare diseases informing common health issues, the identification of SORD-associated neuropathy may have broader implication to the field of diabetic neuropathy and retinopathy. Diabetes represents the most frequent cause of neuropathy in Western countries, affecting 30 - 60% of diabetic patients and 20–30 million people world-wide (38,39). Its pathogenesis is exceptionally complex and available treatments are mostly symptomatic. Increased polyol pathway flux has been reported to cause osmotic damage and oxidative stress to retinal cells, including neurons, Müller glia, pericytes, and vascular endothelial cells(40). Aberrant retinal sorbitol accumulation can lead to microvascular damage and subsequent neovascularization(41). However, the direct impact of sorbitol accumulation on photoreceptor neurons is not well characterized. Our fly models of SORD deficiency show the age-dependent formation of vacuole-like structures and reduced synaptic proteins, indicating that an increased sorbitol level in the retina can have a direct detrimental effect on the photoreceptor neurons and contribute to retinal phenotypes in diabetic retinopathy. Further elucidation of the process leading to nerve degeneration in the constituent absence of SORD will hopefully translate into a better understanding of the composite mechanisms underlying onset and progression of diabetic neuropathy and retinopathy.

REFERENCES

1. Rossor AM, Tomaselli PJ, Reilly MM. Recent advances in the genetic neuropathies. Curr Opin Neurol. 2016;29(5):537–48.

2. Fridman V, Bundy B, Reilly MM, Pareyson D, Bacon C, Burns J, et al. CMT subtypes and disease burden in patients enrolled in the Inherited Neuropathies Consortium natural history study: a cross-sectional analysis. J Neurol Neurosurg Psychiatry. 2015 Aug;86(8):873–8.

3. Gonzalez M, Falk MJ, Gai X, Postrel R, Schüle R, Zuchner S. Innovative genomic collaboration using the GENESIS (GEM.app) platform. Hum Mutat. 2015 Oct;36(10):950–6.

4. Hellgren M, Kaiser C, de Haij S, Norberg A, Höög J-O. A hydrogen-bonding network in mammalian sorbitol dehydrogenase stabilizes the tetrameric state and is essential for the catalytic power. Cell Mol Life Sci CMLS. 2007 Dec;64(23):3129–38.

5. Carr AS, Pelayo-Negro AL, Evans MR, Laurà M, Blake J, Stancanelli C, et al. A study of the neuropathy associated with transthyretin amyloidosis (ATTR) in the UK. J Neurol Neurosurg Psychiatry. 2016 Jun;87(6):620–7.

6. 1000 Genomes Project Consortium, Auton A, Brooks LD, Durbin RM, Garrison EP, Kang HM, et al. A global reference for human genetic variation. Nature. 2015 Oct 1;526(7571):68–74.

7. Lek M, Karczewski KJ, Minikel EV, Samocha KE, Banks E, Fennell T, et al. Analysis of protein-coding genetic variation in 60,706 humans. Nature. 2016 18;536(7616):285–91.

8. Lazarin GA, Haque IS, Nazareth S, Iori K, Patterson AS, Jacobson JL, et al. An empirical estimate of carrier frequencies for 400+ causal Mendelian variants: results from an ethnically diverse clinical sample of 23,453 individuals. Genet Med Off J Am Coll Med Genet. 2013 Mar;15(3):178–86.

9. Antonarakis SE. Carrier screening for recessive disorders. Nat Rev Genet. 2019;20(9):549–61.

10. Murphy SM, Herrmann DN, McDermott MP, Scherer SS, Shy ME, Reilly MM, et al. Reliability of the CMT neuropathy score (second version) in Charcot-Marie-Tooth disease. J Peripher Nerv Syst JPNS. 2011 Sep;16(3):191–8.

11. Johansson K, El-Ahmad M, Kaiser C, Jörnvall H, Eklund H, Höög J, et al. Crystal structure of sorbitol dehydrogenase. Chem Biol Interact. 2001 Jan 30;130–132(1–3):351–8.

12. Lindstad RI, Teigen K, Skjeldal L. Inhibition of sorbitol dehydrogenase by nucleosides and nucleotides. Biochem Biophys Res Commun. 2013 May 31;435(2):202–8.

13. Luque T, Hjelmqvist L, Marfany G, Danielsson O, El-Ahmad M, Persson B, et al. Sorbitol dehydrogenase of Drosophila. Gene, protein, and expression data show a two-gene system. J Biol Chem. 1998 Dec 18;273(51):34293–301.

14. Bellen HJ, Levis RW, He Y, Carlson JW, Evans-Holm M, Bae E, et al. The Drosophila gene disruption project: progress using transposons with distinctive site specificities. Genetics. 2011 Jul;188(3):731–43.

15. Bausenwein B, Dittrich AP, Fischbach KF. The optic lobe of Drosophila melanogaster. II. Sorting of retinotopic pathways in the medulla. Cell Tissue Res. 1992 Jan;267(1):17–28.

16. Kikkawa R, Hatanaka I, Yasuda H, Kobayashi N, Shigeta Y, Terashima H, et al. Effect of a new aldose reductase inhibitor, (E)-3-carboxymethyl-5-[(2E)-methyl-3-phenylpropenylidene]rhodanine (ONO-2235) on peripheral nerve disorders in streptozotocin-diabetic rats. Diabetologia. 1983 Apr;24(4):290–2.

17. Matsumoto T, Ono Y, Kuromiya A, Toyosawa K, Ueda Y, Bril V. Long-term treatment with ranirestat (AS-3201), a potent aldose reductase inhibitor, suppresses diabetic neuropathy and cataract formation in rats. J Pharmacol Sci. 2008 Jul;107(3):340–8.

18. Ramirez MA, Borja NL. Epalrestat: an aldose reductase inhibitor for the treatment of diabetic neuropathy. Pharmacotherapy. 2008 May;28(5):646–55.

19. Hao W, Tashiro S, Hasegawa T, Sato Y, Kobayashi T, Tando T, et al. Hyperglycemia Promotes Schwann Cell De-differentiation and De-myelination via Sorbitol Accumulation and Igf1 Protein Down-regulation. J Biol Chem. 2015 Jul 10;290(28):17106–15.

20. Grewal AS, Bhardwaj S, Pandita D, Lather V, Sekhon BS. Updates on Aldose Reductase Inhibitors for Management of Diabetic Complications and Non-diabetic Diseases. Mini Rev Med Chem. 2016;16(2):120–62.

21. Chalk C, Benstead TJ, Moore F. Aldose reductase inhibitors for the treatment of diabetic polyneuropathy. Cochrane Database Syst Rev. 2007 Oct 17;(4):CD004572.

22. Polydefkis M, Arezzo J, Nash M, Bril V, Shaibani A, Gordon RJ, et al. Safety and efficacy of ranirestat in patients with mild-to-moderate diabetic sensorimotor polyneuropathy. J Peripher Nerv Syst JPNS. 2015 Dec;20(4):363–71.

23. Sekiguchi K, Kohara N, Baba M, Komori T, Naito Y, Imai T, et al. Aldose reductase inhibitor ranirestat significantly improves nerve conduction velocity in diabetic polyneuropathy: A randomized double-blind placebo-controlled study in Japan. J Diabetes Investig. 2019 Mar;10(2):466–74.

24. Züchner S, Mersiyanova IV, Muglia M, Bissar-Tadmouri N, Rochelle J, Dadali EL, et al. Mutations in the mitochondrial GTPase mitofusin 2 cause Charcot-Marie-Tooth neuropathy type 2A. Nat Genet. 2004 May;36(5):449–51.

25. De Vos M, Hayward BE, Picton S, Sheridan E, Bonthron DT. Novel PMS2 pseudogenes can conceal recessive mutations causing a distinctive childhood cancer syndrome. Am J Hum Genet. 2004 May;74(5):954–64.

26. Rumsby G, Carroll MC, Porter RR, Grant DB, Hjelm M. Deletion of the steroid 21-hydroxylase and complement C4 genes in congenital adrenal hyperplasia. J Med Genet. 1986 Jun;23(3):204–9.

27. Chen J-M, Cooper DN, Chuzhanova N, Férec C, Patrinos GP. Gene conversion: mechanisms, evolution and human disease. Nat Rev Genet. 2007 Oct;8(10):762–75.

28. Harel T, Yoon WH, Garone C, Gu S, Coban-Akdemir Z, Eldomery MK, et al. Recurrent De Novo and Biallelic Variation of ATAD3A, Encoding a Mitochondrial Membrane Protein, Results in Distinct Neurological Syndromes. Am J Hum Genet. 2016 Oct 6;99(4):831–45.

29. Lupski JR, de Oca-Luna RM, Slaugenhaupt S, Pentao L, Guzzetta V, Trask BJ, et al. DNA duplication associated with Charcot-Marie-Tooth disease type 1A. Cell. 1991 Jul 26;66(2):219–32.

30. Schmidt RE, Dorsey DA, Beaudet LN, Plurad SB, Parvin CA, Yarasheski KE, et al. Inhibition of sorbitol dehydrogenase exacerbates autonomic neuropathy in rats with streptozotocin-induced diabetes. J Neuropathol Exp Neurol. 2001 Dec;60(12):1153–69.

31. Schmidt RE, Dorsey DA, Beaudet LN, Parvin CA, Yarasheski KE, Smith SR, et al. A potent sorbitol dehydrogenase inhibitor exacerbates sympathetic autonomic neuropathy in rats with streptozotocin-induced diabetes. Exp Neurol. 2005 Apr;192(2):407–19.

32. Obrosova IG. Increased sorbitol pathway activity generates oxidative stress in tissue sites for diabetic complications. Antioxid Redox Signal. 2005 Dec;7(11–12):1543–52.

33. Sango K, Suzuki T, Yanagisawa H, Takaku S, Hirooka H, Tamura M, et al. High glucose-induced activation of the polyol pathway and changes of gene expression profiles in immortalized adult mouse Schwann cells IMS32. J Neurochem. 2006 Jul;98(2):446–58.

34. Holmes RS, Duley JA, Hilgers J. Sorbitol dehydrogenase genetics in the mouse: a “null” mutant in a “European” C57BL strain. Anim Blood Groups Biochem Genet. 1982;13(4):263–72.

35. Lee AY, Chung SK, Chung SS. Demonstration that polyol accumulation is responsible for diabetic cataract by the use of transgenic mice expressing the aldose reductase gene in the lens. Proc Natl Acad Sci U S A. 1995 Mar 28;92(7):2780–4.

36. Ng TF, Lee FK, Song ZT, Calcutt NA, Lee AY, Chung SS, et al. Effects of sorbitol dehydrogenase deficiency on nerve conduction in experimental diabetic mice. Diabetes. 1998 Jun;47(6):961–6.

37. Ruff JS, Suchy AK, Hugentobler SA, Sosa MM, Schwartz BL, Morrison LC, et al. Human-relevant levels of added sugar consumption increase female mortality and lower male fitness in mice. Nat Commun. 2013;4:2245.

38. Callaghan BC, Cheng HT, Stables CL, Smith AL, Feldman EL. Diabetic neuropathy: clinical manifestations and current treatments. Lancet Neurol. 2012 Jun;11(6):521–34.

39. Dyck PJ, Kratz KM, Karnes JL, Litchy WJ, Klein R, Pach JM, et al. The prevalence by staged severity of various types of diabetic neuropathy, retinopathy, and nephropathy in a population-based cohort: the Rochester Diabetic Neuropathy Study. Neurology. 1993 Apr;43(4):817–24.

40. Stewart M. Pathophysiology of diabetic retinopathy. In: Diabetic Retinopathy Current Pharmacologic Treatment and Emerging Strategies. Springer; 2017.

41. Lorenzi M. The polyol pathway as a mechanism for diabetic retinopathy: attractive, elusive, and resilient. Exp Diabetes Res. 2007;2007:61038.

42. Li L, Ye Y, Pan L, Zhu Y, Zheng S, Lin Y. The induction of trehalose and glycerol in Saccharomyces cerevisiae in response to various stresses. Biochem Biophys Res Commun. 2009 Oct 2;387(4):778–83.

Acknowledgements

This project was supported by NINDS (R01NS075764 to S.Z. and M.S.), NIH (R21GM119018 to R.G.Z;), NCATS (U54NS065712 to M.S), CMT Association, Muscular Dystrophy Association, the European Union's Horizon 2020 research and innovation program under the ERA-NET Cofund action N° 643578 under the frame of the E-Rare-3 network PREPARE (01GM1607 to M. S; and unfunded to S.Z.) and by the grant 779257 "Solve-RD" (to R.S. and M.S., M.R. and H.H). The project received further support from the 'Bundesministerium für Bildung und Forschung' (BMBF) via funding for the TreatHSP consortium (01GM1905 to R. S.) and the National Institutes of Health (grant 5R01NS072248 to R. S. and S. Z.), the Austrian Science Fund (FWF, P27634FW to MA-G), National Natural Science Foundation of China (81771366). AC, HH and MMR thank the MRC, Wellcome Trust, MDA, MD UK and NIHR UCLH BRC for grant support. A.M.R. is funded by a Wellcome Trust Postdoctoral Fellowship for Clinicians (110043/Z/15/Z). M.L. received support from NIHR UCLH BRC. D.N.H. receives grant support through NIH U54 NS065712-09, the Muscular Dystrophy Association, the Friedreich's Ataxia Alliance, and Voyager Pharmaceuticals. We would like to thank Dr Mustafa Tekin for kindly providing DNA from Turkish healthy controls.

Author contributions:

Conceptualization, A.C., S.Z.

Funding acquisition, S.Z, M.E.S, M.M.R., H.H., R.S., M.S.

Investigation, A.C., Y.Z., A.R., S.N., S.C., M.P., E.B., G.Z., S.Z.

Resources, A.C., Y.Z., A.R., S.N., S.C., L.A., A.A.-A, M. A.-G., C.J.B., Y.B., D.B., E.B., J.D., M.C.D., S.M.E.F., A.A.F., E.G., M.A.A.E.H., S.E.H., N.H., H.H., R.I., A.K., M.L., Z.L., S.M., T.M., F.M., E.M., D.P., M.P., C.P., E.P., A.M.R., L.S., S.S.S., R.S., J.S., T.S., M.S., B.T., F.T., S.T., J.V., R.Z., D.H., M.M.R., M.E.S., G.Z., S.Z.

Supervision, S.Z., G.Z.

Writing–original draft, A.C., Y.Z., A.R., G.Z., S.Z.

All authors contributed to revising the manuscript.

Competing interests: The authors declare no financial or commercial conflicts of interest.

Data and materials availability: All data described in this paper are present either in the main text or in the supplementary materials

FIGURES

Figure 1. Biallelic mutations in *SORD* cause autosomal recessive dHMN/CMT2. A) Representative pedigrees of dHMN/CMT2 families carrying biallelic mutations in *SORD*. A full set of pedigrees is provided in **Supplementary Fig. 1**. The squares indicate males and the circles females. The diagonal lines are used for deceased individuals. Patients are indicated with filled shapes. “+” indicate presence and “-“ absence of mutant allele **B)** Schematic diagram showing all exons, introns and untranslated regions (UTRs) of *SORD* based on NCBI reference sequence NM_003104.6. The gray and white boxes represent the coding sequence and UTRs of *SORD*, respectively. The variants identified in the CMT families considered in the present study map throughout the coding region of the gene. The nonsense variant c.753delG; p.Ala253GlnfsTer27 on exon 7, highlighted, was identified at particular high frequency. **C)** Distribution of mutations across SORD protein domains. **D)** SORD protein orthologs alignments showing that the four missense substitutions identified in dHMN/CMT2 families in this study are located at highly conserved residues across species from human to Drosophila (*Sodh2*). **E)** Schematic representation *of SORD* and its paralogue *SORD2P*, arisen from the duplication of *SORD* within a 0.5 Mb region on chromosome 15. Highly homologous exonic regions between *SORD* and *SORD2P* are connected by dotted lines **F)** Magnification of the nucleotide sequence of a highly homologous region in exon 7 in SORD (reverse strand) and *SORD2P* (forward strand). Nucleotides differing in *SORD2P* from *SORD* are highlighted in yellow, including a C deletion in *SORD2P*. Representative electropherograms show that the c.753delG; p.Ala253GlnfsTer27 *SORD* variant is found in a homozygous state in dHMN/CMT2 patients (red box, lower plot) and in a heterozygous state in available parents (red box, upper plot), and is absent in biallelic state from healthy controls (grey box), but it is fixed in *SORD2P* (blue box).

Figure 1.

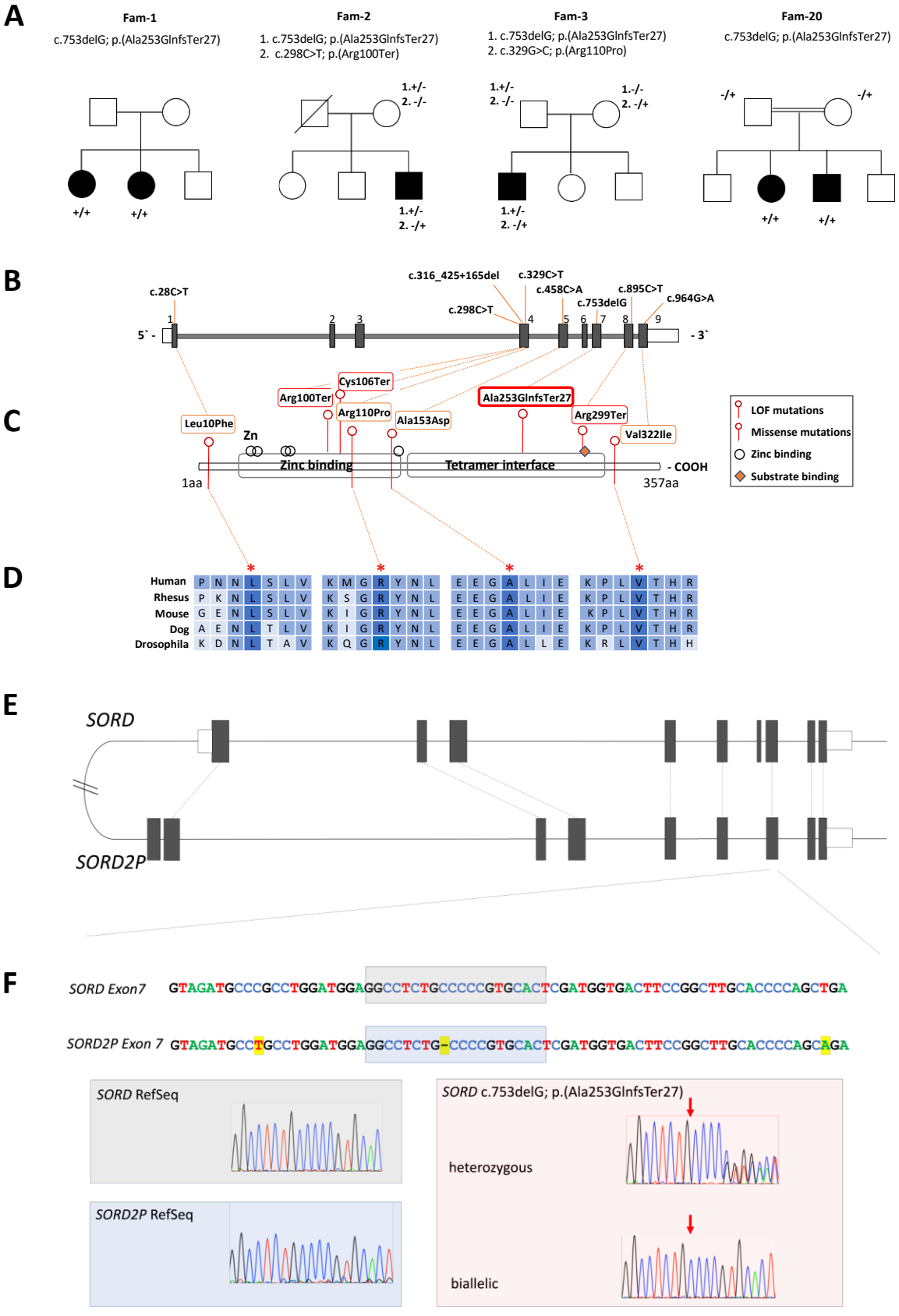
A
Fam-1
c.753delG; p.(Ala253GlnfsTer27)
+/+
+/+
Fam-2
1. c.753delG; p.(Ala253GlnfsTer27)
2. c.298C>T; p.(Arg100Ter)
1.+/-
2. -/-
1.+/-
2. -/+
Fam-3
1. c.753delG; p.(Ala253GlnfsTer27)
2. c.329G>C; p.(Arg110Pro)
1.+/-
2. -/-
1.-/-
2. -/+
1.+/-
2. -/+
Fam-20
c.753delG; p.(Ala253GlnfsTer27)
-/+
-/+
+/+
+/+
B
c.28C>T
c.316_425+165del
c.329C>T
c.458C>A
c.298C>T
c.753delG
c.895C>T
c.964G>A
5` -
- 3`
C
Cys106Ter
Arg100Ter
Arg110Pro
Ala153Asp
Ala253GlnfsTer27
Arg299Ter
Leu10Phe
Val322Ile
Zn
Zinc binding
Tetramer interface
1aa
- COOH
357aa
LOF mutations
Missense mutations
Zinc binding
Substrate binding
D
Human
Rhesus
Mouse
Dog
Drosophila
E
SORD
SORD2P
F
SORD Exon7 GTAGATGCCCGCCTGGATGGAGGCCTCTGCCCCCGTGCACTCGATGGTGACTTCCGGCTTGCACCCCAGCTGA
SORD2P Exon 7 GTAGATGCCTGCCTGGATGGAGGCCTCTG-CCCCGTGCACTCGATGGTGACTTCCGGCTTGCACCCCAGCAGA
SORD RefSeq
SORD2P RefSeq
SORD c.753delG; p.(Ala253GlnfsTer27)
heterozygous
biallelic

Figure 2. Decreased SORD expression and sorbitol accumulation in patients' fibroblasts. **A)** Schematic representation of the two-step polyol pathway converting glucose to fructose **B)** Representative immunoblot showing the levels of SORD and tubulin protein in four healthy controls (lane 1-4), four patients carrying homozygous p.Ala253GlnfsTer27 alleles (lane 5-8), one compound heterozygous p.Ala253GlnfsTer27/ p.Arg299Ter patient (lane 9), and two heterozygous carriers of p.Ala253GlnfsTer27 (lane 10-11). **C)** Levels of intracellular sorbitol was measured by ultra-performance liquid chromatography and normalised to protein content in cultured fibroblasts from five unrelated healthy controls and five patients carrying biallelic p.Ala253GlnfsTer27 mutations in *SORD*. **D)** Fasting sorbitol level in serum from ten unrelated healthy controls and ten patients carrying biallelic p.Ala253GlnfsTer27 mutations in SORD. The graphs show the mean ± s.d. and data distribution (dots), and the p-value of two-tailed t-tests comparing SORD protein and sorbitol levels across groups - * p<0.05, ** p<0.01, and *** p<0.001. All experiments were twice repeated independently.

Figure 2

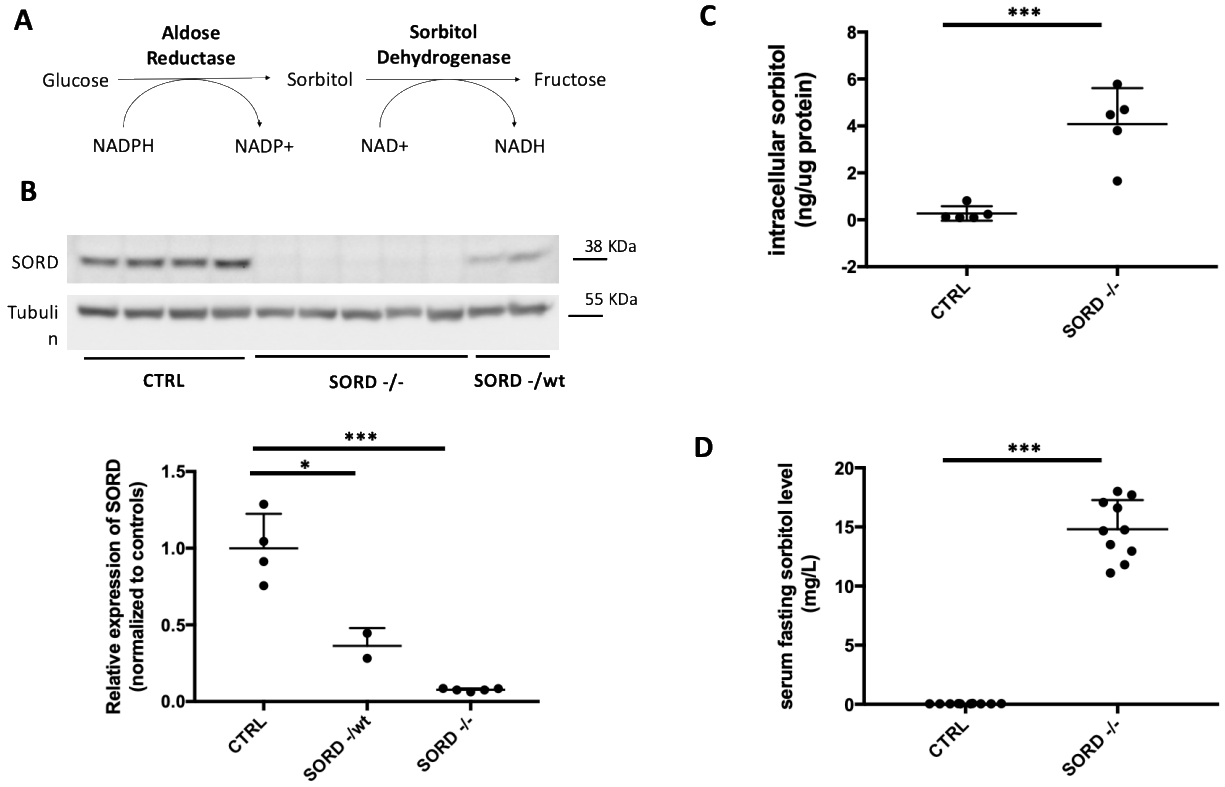

Figure 3. Loss of *Drosophila* Sodh2 causes age-dependent synaptic degeneration. A) 3D structure of the *Drosophila* visual system stained with Horseradish peroxidase (HRP, green; marks neuronal membranes) and bruchpilot (BRP, magenta; marks synaptic active zones), showing the lamina, medulla, and lobula. The xy- and xz-planes showing the photoreceptor terminals and lamina neurons are indicated. **B)** Optical sections of the laminae of yw control flies at 2 DAE, stained with HRP (green) and BRP (magenta). The organized lamina cartridges and columnar photoreceptor neurons are shown in the xy-plane and xz-plane, respectively. **C)** Optical sections of the laminae at the level of the terminals of $Sodh2^{MB01265/MB01265}$ homozygous flies at 2 DAE and 10 DAE, stained with HRP (green) and BRP (magenta). Yellow arrowheads indicate the lamina vacuole-like structures that correspond to missing terminals. The areas outlined by yellow boxes are shown at higher magnification. The intensity of BRP is indicated using a red spectrum. Dotted lines indicate the area of lamina vacuole-like structures. Scale bar: 30 μm. **D)** Quantification number and size of the vacuole-like structures. A total of 8 laminae of each group were quantified. Data are presented as mean ± s.d. Statistical analysis was performed using two-way ANOVA followed by post-hoc Tukey's multiple comparison test. *p<0.05, **p<0.01, ****p<0.0001. **E-F)** Locomotor activity of control flies (yw) and $Sodh2^{MB01265/MB01265}$ (**E**) or Sodh1 and Sodh2 pan-neuronal double knockdown (RNAi) (**F**) flies. n=10 in each group. Data are presented as mean ± s.d. Statistical analysis was performed using two-way ANOVA followed by post-hoc Tukey's multiple comparison test. ****p<0.0001

Figure 3

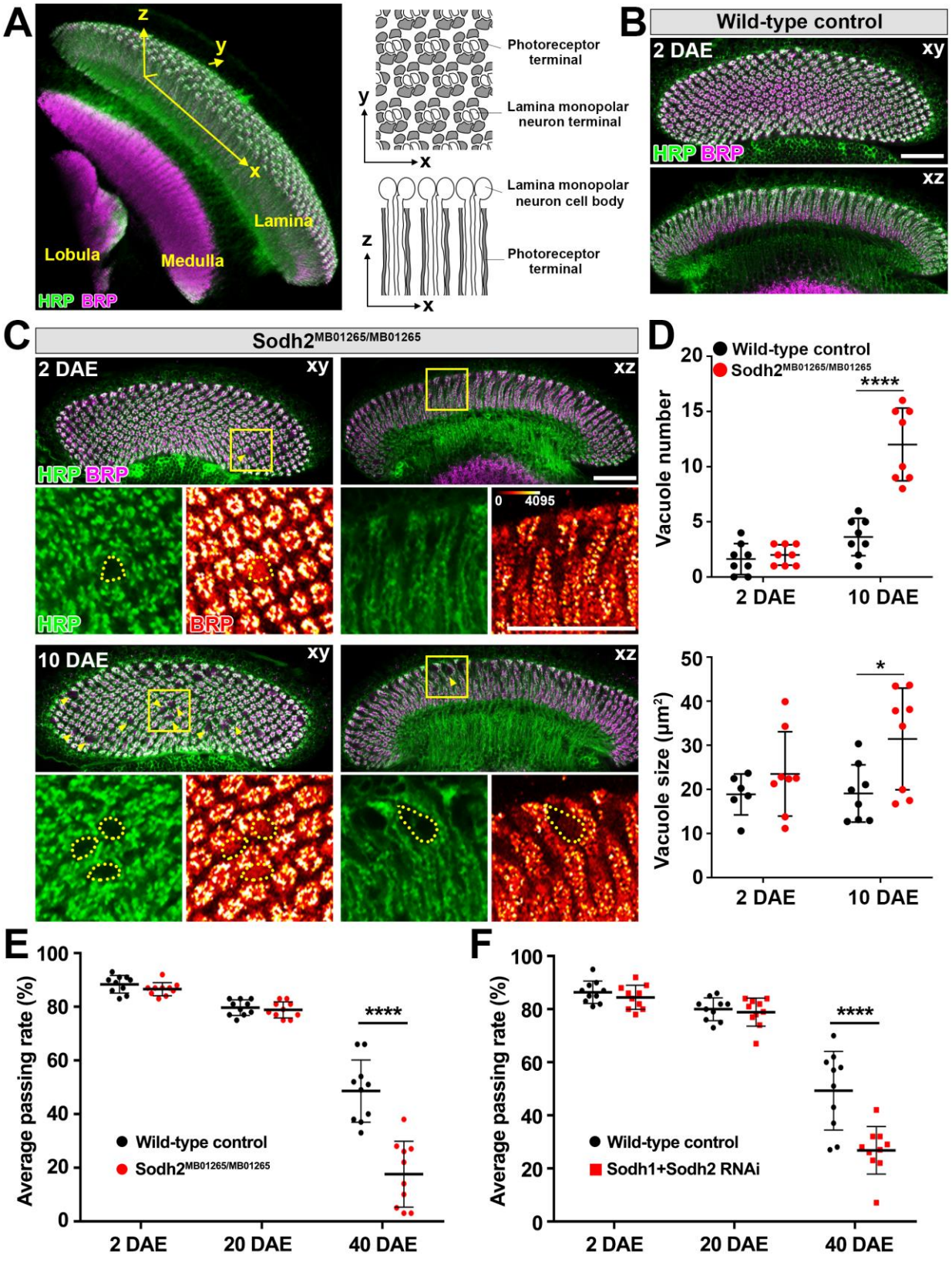
A
z
y
x
Lamina
Lobula
Medulla
HRP BRP
Photoreceptor terminal
Lamina monopolar neuron terminal
Lamina monopolar neuron cell body
Photoreceptor terminal
B
Wild-type control
2 DAE
xy
xz
HRP BRP
C
Sodh2MB01265/MB01265
2 DAE
10 DAE
HRP
BRP
0
4095
D
Wild-type control
Sodh2MB01265/MB01265
Vacuole number
Vacuole size (µm²)
****
*
2 DAE
10 DAE
E
Average passing rate (%)
Wild-type control
Sodh2MB01265/MB01265
2 DAE
20 DAE
40 DAE
F
Wild-type control
Sodh1+Sodh2 RNAi

Figure 4. Treatment with aldose reductase inhibitors Epalrestat and Ranirestat decrease sorbitol levels and prevent functional losses. A) Intracellular sorbitol levels were measured by ultra-performance liquid chromatography and normalized to protein content in fibroblasts from healthy controls (N=5, circle dots) and patients carrying biallelic nonsense mutations in *SORD* (N=5, square dots) after three days of treatment with 100 μM Epalrestat (blue dots), 10 μM Ranirestat (green dots) or DMSO (red dots). **B)** Sorbitol level were measured in brain/head homogenates and normalized to protein concentration from wild-type (yw, empty circle dots) and *Sodh2*$^{MB01265/MB01265}$ (full circle dots) *Drosophilae* at 10 days after eggs enclosure (DAE). *Sodh2*$^{MB01265/MB01265}$ were fed Epalrestat (blue dots) or Ranirestat (green dots) at a final concentration of 80 μg/ml, or DMSO (red dots). The graphs show the mean ± s.d. A two-tailed t-test was performed to compare sorbitol level. **p<0.01, ***p<0.001.. All experiments were repeated independently twice with similar results. **C)** Locomotor activity of control flies (*yw*) feeding with DMSO (black dots), *Sodh2*$^{MB01265/MB01265}$ flies feeding with DMSO (red dots), 80 μg/ml Epalrestat (blue dots), or 80 μg/ml Ranirestat (green dots). N=10 in each group. Data are presented as mean ± s.d. Statistical analysis was performed using two-way ANOVA followed by post-hoc Tukey's multiple comparison test. * p<0.05, *** p<0.001 **D-F)** Laminae of *Sodh2*$^{MB01265/MB01265}$ homozygous flies at 10 DAE and 40 DAE fed with DMSO (**D**), 80 μg/ml Epalrestat (**E**), or 80 μg/ml Ranirestat (**F**) were stained with HRP (green) and BRP (magenta). Yellow arrowheads indicate the lamina vacuole-like structures. The areas outlined by yellow boxes are shown at higher magnification. The intensity of BRP is indicated using a red spectrum. Dotted lines indicate the area of lamina vacuole-like structures. Scale bar: 30 μm. **G**) Quantification number and size of the vacuole-like structures (**D-F**) (N=3). Data are presented as mean ± s.d. Statistical analysis was performed using two-way ANOVA followed by post-hoc Tukey's multiple comparison test. *p<0.05, **p<0.01.

Figure 4

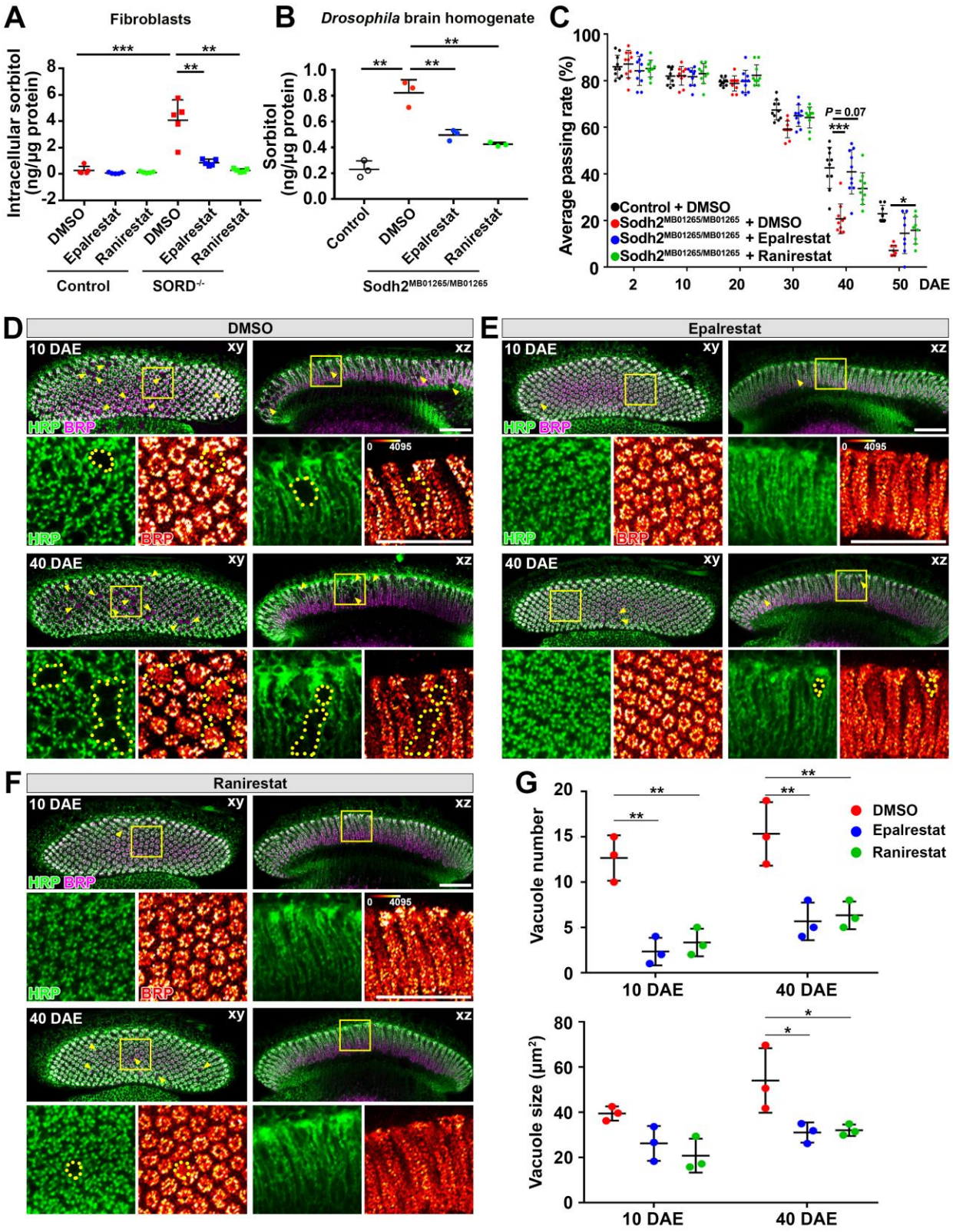
A
Fibroblasts
Intracellular sorbitol (ng/µg protein)
DMSO
Epalrestat
Ranirestat
Control
SORD-/-
B
Drosophila brain homogenate
Sorbitol (ng/µg protein)
Control
DMSO
Epalrestat
Ranirestat
Sodh2MB01265/MB01265
C
Average passing rate (%)
P = 0.07
Control + DMSO
Sodh2MB01265/MB01265 + DMSO
Sodh2MB01265/MB01265 + Epalrestat
Sodh2MB01265/MB01265 + Ranirestat
DAE
D
DMSO
E
Epalrestat
F
Ranirestat
10 DAE
40 DAE
xy
xz
HRP BRP
HRP
BRP
G
Vacuole number
Vacuole size (µm²)
DMSO
Epalrestat
Ranirestat
10 DAE
40 DAE

TABLES

Table 1. Clinical features of patients affected by hereditary neuropathy and carrying the biallelic mutations in SORD

	N=45
Male	32 (71%)
Age of onset (years)	17 ± 8 (2-40)
Age at examination (years)	34 ± 13 (15-70)
Family history of neuropathy	14 (31%)
CMT subtype	
CMT2	23 (51%)
dHMN	18 (40%)
CMT intermediate	4 (9%)
Foot deformities	31 (69%)
Upper limb weakness	
Proximal muscle groups	0/44 (0%)
Distal muscle groups	26/44 (59%)
Lower limb weakness	
Proximal muscle groups	2/44 (5%)
Distal muscle groups	43/44 (98%)
Prominent involvement of foot plantar flexion*	15/37 (41%)
Reduced vibratory sensation	17/40 (42%)
Reduced pinprick superficial sensation	13/39 (33%)
Disease severity	
Mild	30 (67%)
Moderate	14 (31%)
Severe	1 (2%)
Use of ankle-foot orthoses (AFOs)	19 (42%)
Other walking aids	2 (4%)
Nerve conduction study	
Reduced motor conduction velocity	11/42 (26%)
Reduced sensory action potentials	26/40 (65%)

Categorical data are expressed as N (%) if data is available in all individuals or N/number individuals considered (%). Continuous variables are expressed as mean ± standard deviation (min-max). CMT, Charcot-Marie-Tooth, CMTNSv2, CMT Neuropathy Score, version 2; dHMN, distal hereditary motor neuropathy, * foot plantar flexion equal or weaker than foot dorsal flexion.

MATERIAL AND METHODS

Patients

For the initial discovery study, we enrolled 598 individuals who previously underwent whole exome sequencing (WES) or whole-genome sequencing (WGS) with a clinical diagnosis of CMT, collected through the collaborative initiative Inherited Neuropathy Consortium, which recruit patients from 15 sites in the United States and the United Kingdom. Additional 400 cases with a clinical diagnosis of sporadic or recessive dHMN or CMT2 and negative for the known genetic defects associated with the disease were collected across additional centres in the United Kingdom, Italy, Kuwait, Saudi Arabia and China. The study has received ethical approval (INC 6602) and all subjects gave written informed consent to participate. The study has complied with all relevant ethical regulations.

Disease severity was scored using the previously validated Charcot-Marie-Tooth Neuropathy Score (CMTNSv2) or CMT Examination Score (CMTESv2) (8) and cases were divided into mild (CMTNS 0 to 10 or CMTES 0 to 7), moderate (CMTNS 11 to 20 or CMTES 8 to 16 and severe (CMTNS 21 to 36 or CMTES 17 to 28). In cases for which CMTNS or CMTES had not been collected, disease was considered mild if walking was possible without aid, moderate if walking was possible with foot orthosis or ankle dorsiflexion was <3 MRC grade, and severe if patients needed a walking aid, such as a stick or a wheelchair.

WES and WGS:

WES was performed in 598 index individuals from sporadic and recessive CMT and dHMN families. The SureSelect Human All Exon 50 MB Kit (Agilent) was used for in-solution enrichment, and the HiSeq 2500 instrument (Illumina) was used to produce about 120 bp paired-end sequence reads. The Burrows-Wheeler aligner, and Freebayers were used to align sequence reads and call variants. Final data were uploaded into GENESIS software for analysis (genesis-app.com). A filtering approach to search for families sharing the same homozygous variants were applied across all exomes in the database. Variants were prioritized based on segregation, minor allele frequency (<0.0001 in the 1000 Genomes Project(6), NHLBI GO Exome Sequencing project (Exome Variant Server, NHLBI GO Exome Sequencing Project (ESP), Seattle, WA (URL: http://evs.gs.washington.edu/EVS/) (September 2017), or gnomAD (7),

PCR and Sanger sequencing of SORD and SORD2P

Coding exons and flanking introns of *SORD* and exon 7 of SORD2P were amplified from genomic DNA by PCR followed by Sanger Sequencing. If necessary, an internal distinct primer was used for sequencing. Primers sequences, concentrations and PCR thermocycling conditions are provided in Supplementary Table 1. Sanger sequencing was performed by Eurofins Genomics USA (Louisville, Kentucky, USA) or Source Bioscience (Cambridge, UK).

Fibroblasts cultures

A skin biopsy was performed for fibroblasts culture in four patients carrying biallelic c.753delG; p.Ala253GlnfsTer27 variants (Fam 4 II, Fam 7, Fam 9 and Fam 16) and one case carrying one heterozygous c.753delG; p.Ala253GlnfsTer27 variant and one additional nonsense c.895C>T; p.(Arg299Ter) variant, two unaffected carriers of the c.753delG; p.Ala253GlnfsTer27 variant (Fam 4 I-1 and I-2) and five age- and gender-matched controls.

Fibroblasts were cultured in Dulbecco's Modified Eagle Medium (ThermoFisher) supplemented with 10% fetal bovine serum (FBS), penicillin and streptomycin (Gibco). Cells were grown in 5% CO2 at 37°C in a humidified incubator. Asynchronous cell cultures were grown to approximately 80% confluency, then treated with epalrestat (100μM), ranirestat (10μM) or dimethyl sulfoxide (DMSO) for 72 hours. The media containing the drugs or DMSO was changed every 24 hours.

Western blotting

Fibroblasts were lysed in RIPA buffer (ThermoFisher) containing protease inhibitors (Roche) and sonicated for 5 minutes with the Bioruptor sonication device (Diagenode). Cell lysates were centrifuged at 13,000 x g for 10 minutes at 4 °C, and the supernatant was collected for protein quantification (Pierce BCA Protein Assay Kit). 30 µg of protein sample was mixed with Bolt™ LDS Sample Buffer and Sample Reducing Agent (ThermoFisfer) and heated at 90°C for 5 min. Samples were loaded on Bolt® 4–12% Bis-Tris Plus mini-gel followed by transfer into a nitrocellulose membrane (Bio-Rad). Membrane was blocked with 5% non-fat milk and incubated with anti-SORD (1:1000 dilution, ab189248, Abcam) antibody for 2 hours, washed with TBS containing 0.01% Tween 20 (Bio-Rad) and incubated with a peroxidase-conjugated anti-rabbit antibody (1:2500 dilution, Cat. #7074, Cell Signaling). Membrane was subsequently incubated with monoclonal antibody against tubulin (1:1000 dilution, Santa Cruz) and secondary anti-mouse antibody (1:2500 dilution, Cat. #7076, Cell Signaling). Chemoluminescence detection was performed with the SuperSignal™ West Pico PLUS Chemiluminescent Substrate and imaged with the FluorChem E (ProteinSimple).

Sorbitol measurement in human fibroblast lisates and serum

Sorbitol determination from lysates of human fibroblast was done in ultra performance liquid chromatography-tandem mass spectrometry (UPLC-MS/MS) (Waters Acquity UPLC & TQD mass spectrometer - Waters, Milford, MA, USA). Fibroblasts were collected and lysed as described in Western blotting section, but in the absence of proteinase inhibitor, which contains mannitol, a sorbitol enantiomer which can interfere with UPLC-MS/MS sorbitol determination. Lysate samples underwent protein precipitation with acetonitrile (1:5), ten-time dilution with acetonitrile-water (50/50), and clean up on Oasis HLB cartridges (10 mg/1ml), before injection in UPLC (3µL). UPLC conditions: column, BEH amide 1.7 µm (2.1 x 100mm) at 88°C, eluent A, acetonitrile 90%-water 5%-Isopropanol 5%, eluent B, Acetonitrile 80%-water 20%, gradient elution 0 min., 100%A, 3.6min. 100% B, flow rate, 0.45 ml/min. The retention time of sorbitol was 2.7 min. . Linearity of the method was assessed between 0.25-50 mg/L.MS/MS conditions: interface, electrospray interface in negative ion mode, Multiple Reaction Monitoring acquisition, m/z 180.9 → 88.9 (CV 24, CE 15). The detection limit (signal-to-noise ratio=3) was 0.03 mg/L.

For fasting sorbitol level testing, blood was collected for after overnight fasting (last meal the evening before) in serum separator tubes. Samples were centrifuged at 500g for 10 min, serum was separated and frozen within an hour from blood collection. Sorbitol level was tested by UPLC using a method was adapted from Li et al (42). Conditions were as follows: column, BEH Amide 1.7 µm maintained at 25°C (instead of 45°C); eluent A, 10mM ammonium acetate pH10; eluent B, Acetonitrile. Flow rate, 0.6 ml/min with the same gradient. The retention time of Sorbitol was 6.0 min. MS/MS conditions were the same of fibroblast analysis. Serum samples underwent protein precipitation with cold Methanol (1:5), five time dilution with Acetonitrile-water (50/50) and clean up on Oasis HLB cartridges (10mg/1ml), before injection in UPLC (3µL). Calibration curve was done in serum in sorbitol concentration range 0.1-20 mg/L.

***Drosophila* stocks and experimental procedures**

Unless specified, all the flies were kept on cornmeal-molasses-yeast medium at 25 °C, 65% humidity, with 12 h light/12 h dark cycles. The following fly strains used in this study were obtained from Bloomington *Drosophila* Stock Center: *elav*^{C155}*-GAL4*, *GMR-GAL4*, *Sodh2*^{MB01265}, *UAS-Sodh1 RNAi*, and *UAS-Sodh2 RNAi*. Epalrestat or Ranirestat was dissolved in dimethyl sulfoxide (DMSO) to achieve a stock concentration of 10 mg/ml, and then mixed into 10 ml fly food at a final concentration of 80 µg/ml. Equal amount of DMSO was mixed into the fly food as control. The vials were dried at room temperature for 12 h before feeding.

***Drosophila* lifespan assay and negative geotaxis assay**

For lifespan assay, 100 newly enclosed female flies from each group were collected and placed in vials of 20 individuals. Flies were transferred into new vials every 2 days and the number of dead flies was counted. Survival data was plotted using Kaplan-Meier plot and compared between groups using log-rank test. For the negative geotaxis behavior assay, 10 age-matched female flies were placed in a vial marked with a black line drawn horizontally 8 cm above the bottom. Flies were given 60 min to fully recover from CO_2 anesthesia, then gently tapped onto the bottom and given 10 s to climb. Flies that crossed the 8 cm line were counted. For each vial, this assay was repeated 10 times, and 10 independent vials of each group (a total 100 flies per group) were tested. To minimize observer-expectancy bias, this assay was performed with the examiner masked to the group assignment.

***Drosophila* brain immunostaining, imaging and quantification.**

Fly brains were dissected in phosphate-buffered saline (PBS, pH 7.4), fixed in 4% formaldehyde for 10 min, and washed in PBTX (PBS containing 0.4% v/v Triton X-100) for 3 times (15 mins each). Brains were then incubated with primary mouse anti-BRP antibody (nc82, Developmental Studies Hybridoma Bank) at 1:250 dilution in 0.4% PBTX with 5% normal goat serum at 4°C overnight with gentle shaking. Brains were incubated with Cy3-conjugated anti-mouse secondary antibody (Rockland) and Cy5-conjugated anti-HRP (Jackson ImmunoLab) at 1:250 dilution at 4°C overnight with gentle shaking, followed by 4',6-diamidino-2-phenylindole (DAPI, 1:300, Invitrogen) staining at room temperature for 10 min. Samples were mounted on glass slides with VECTASHIELD Antifade Mounting Medium (Vector Laboratories Inc.). Brain slides were imaged using an Olympus IX81 confocal microscope with 60× oil immersion objective lens with a scan speed of 8.0 μs per pixel and spatial resolution of 1024 × 1024 pixels. Images were processed using FluoView 10-ASW (Olympus). Quantifications of the number, size, and BRP intensity of the vacuole-like structures were carried out using ImageJ/Fiji (version 1.52n). A total of 3 laminae (xy-plane as shown in **Fig. 3B**) of each group were used. For quantification of BRP intensity, 5 different regions of each lamina were chosen.

Statistical analyses

Clinical variables were reported as mean ± standard deviation (s.d.) (min-max) (continuous variables) and percentages (categorical variables). Continuous variables from experimental measurements were compared with two-tailed Student's t test or two-way ANOVA followed by post-hoc Tukey's multiple comparison test, as specified in main text and figures. P values of < 0.05 were considered to be significant.

SUPPLEMENTARY FIGURES

Supplementary Fig. 1. **Pedigrees of families carrying biallelic mutations in *SORD.*** The squares indicate males, the circles females, and the diagonal lines deceased individuals. Patients are indicated with filled shapes. Genotypes are provided when tested by Sanger sequencing.

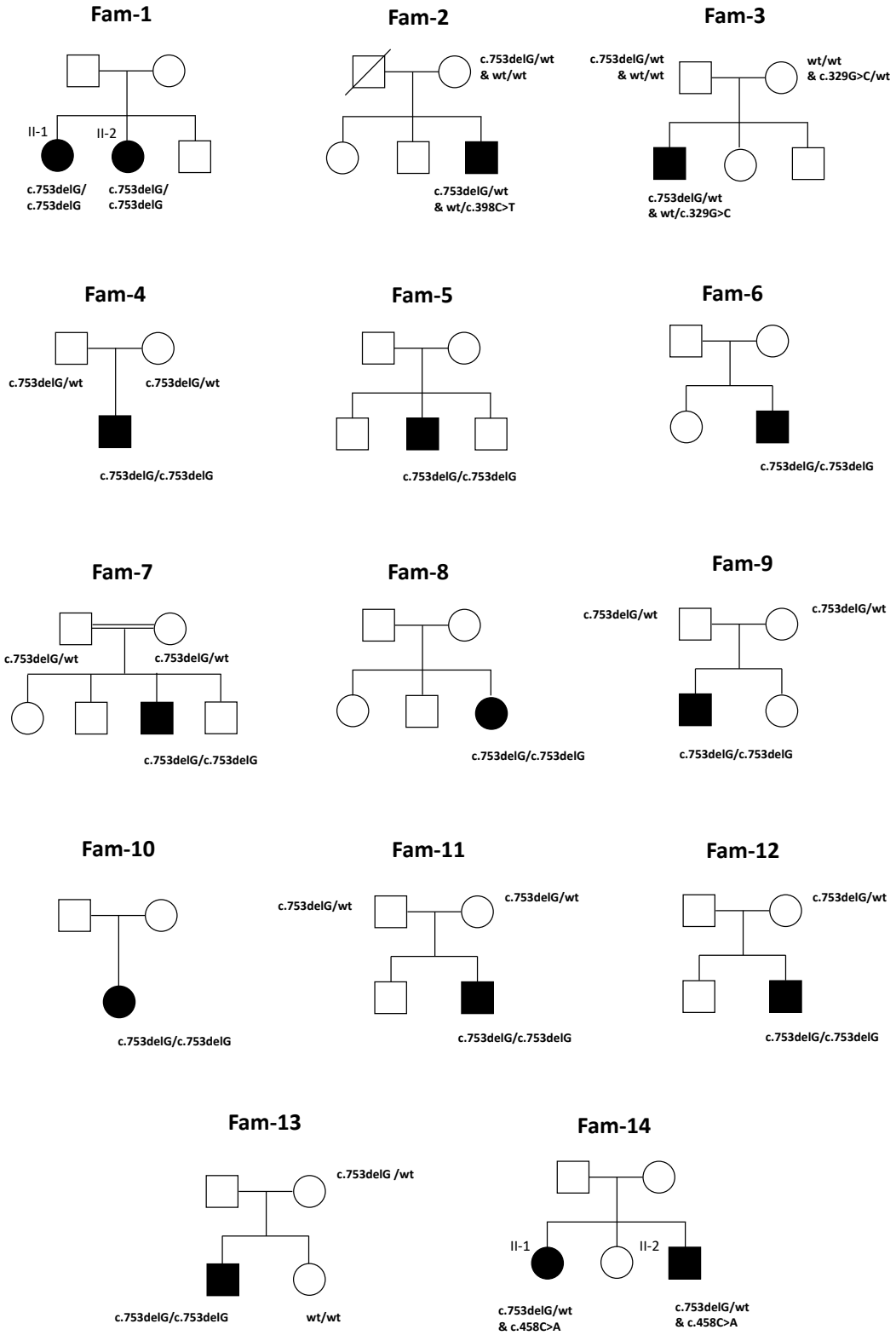
Fam-1
II-1
II-2
c.753delG/
c.753delG
c.753delG/
c.753delG
Fam-2
c.753delG/wt
& wt/wt
c.753delG/wt
& wt/c.398C>T
Fam-3
c.753delG/wt
& wt/wt
wt/wt
& c.329G>C/wt
c.753delG/wt
& wt/c.329G>C
Fam-4
c.753delG/wt
c.753delG/wt
c.753delG/c.753delG
Fam-5
c.753delG/c.753delG
Fam-6
c.753delG/c.753delG
Fam-7
c.753delG/wt
c.753delG/wt
c.753delG/c.753delG
Fam-8
c.753delG/c.753delG
Fam-9
c.753delG/wt
c.753delG/wt
c.753delG/c.753delG
Fam-10
c.753delG/c.753delG
Fam-11
c.753delG/wt
c.753delG/wt
c.753delG/c.753delG
Fam-12
c.753delG/wt
c.753delG/c.753delG
Fam-13
c.753delG /wt
c.753delG/c.753delG
wt/wt
Fam-14
II-1
II-2
c.753delG/wt
& c.458C>A
c.753delG/wt
& c.458C>A

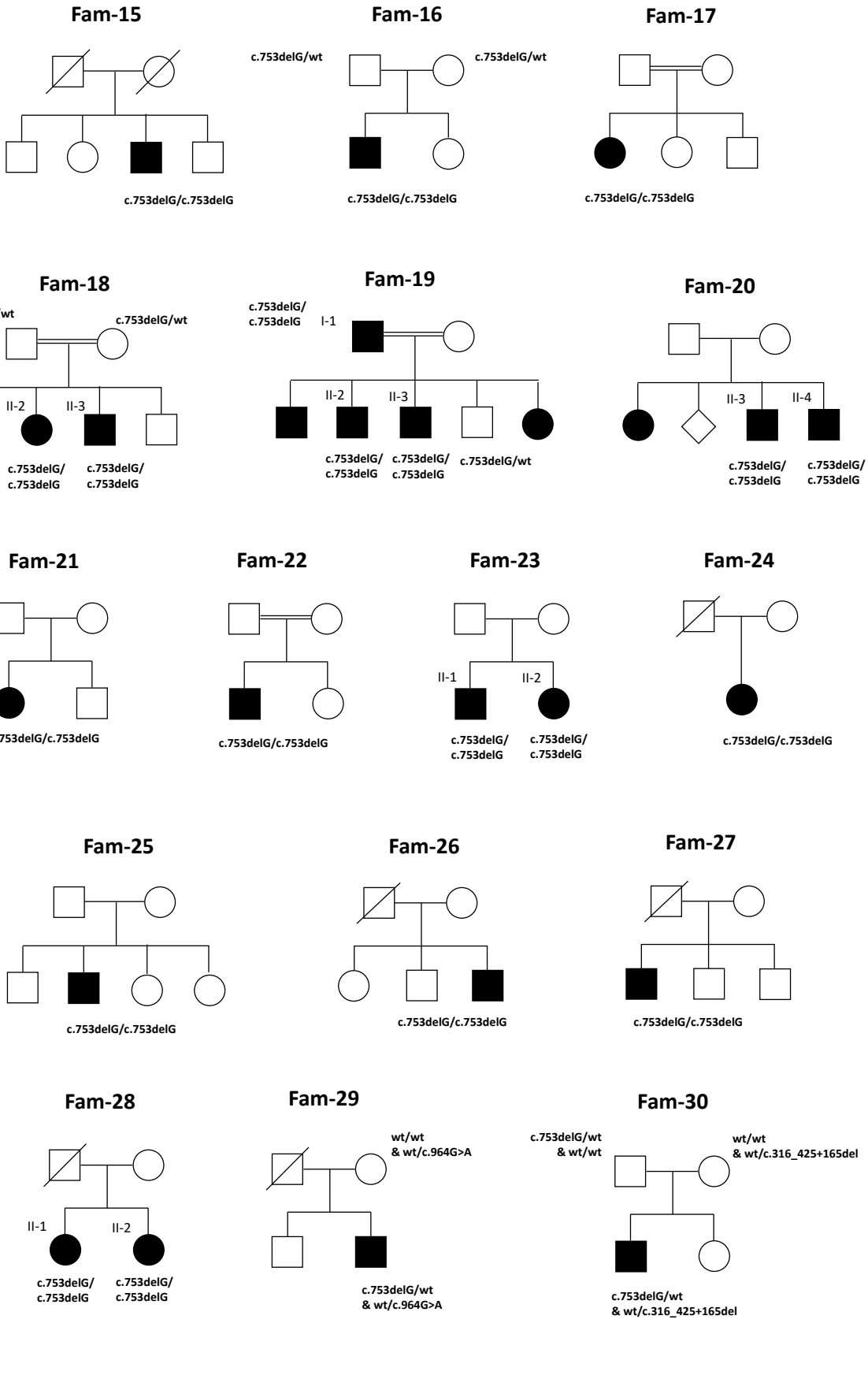
Fam-15
c.753delG/c.753delG
Fam-16
c.753delG/wt
c.753delG/wt
c.753delG/c.753delG
Fam-17
c.753delG/c.753delG
Fam-18
c.753delG/wt
c.753delG/wt
II-2
II-3
c.753delG/
c.753delG
c.753delG/
c.753delG
Fam-19
c.753delG/
c.753delG
I-1
II-2
II-3
c.753delG/
c.753delG
c.753delG/
c.753delG
c.753delG/wt
Fam-20
II-3
II-4
c.753delG/
c.753delG
c.753delG/
c.753delG
Fam-21
c.753delG/c.753delG
Fam-22
c.753delG/c.753delG
Fam-23
II-1
II-2
c.753delG/
c.753delG
c.753delG/
c.753delG
Fam-24
c.753delG/c.753delG
Fam-25
c.753delG/c.753delG
Fam-26
c.753delG/c.753delG
Fam-27
c.753delG/c.753delG
Fam-28
II-1
II-2
c.753delG/
c.753delG
c.753delG/
c.753delG
Fam-29
wt/wt
& wt/c.964G>A
c.753delG/wt
& wt/c.964G>A
Fam-30
c.753delG/wt
& wt/wt
wt/wt
& wt/c.316_425+165del
c.753delG/wt
& wt/c.316_425+165del

Fam-31

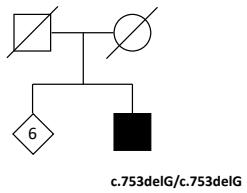

Fam-32

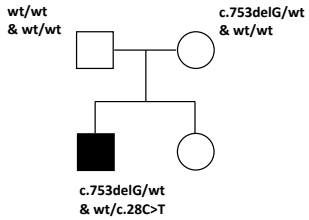

Fam-33

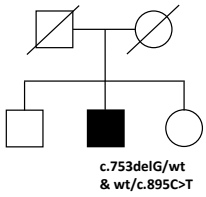

Fam-34 (94719)

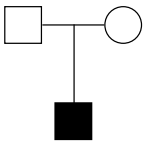

Fam-35 (94853)

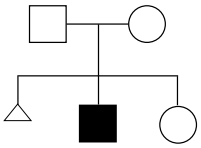

Fam-36

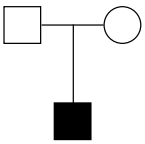

Fam-37

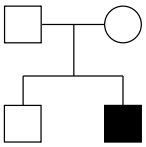

Fam-38

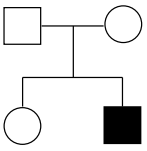

Supplementary Fig. 2. Loss of *Drosophila* Sodh does not affect life span. Life span of control flies (*yw*), *Sodh2*$^{MB01265/MB01265}$ flies, and flies with pan-neuronal knockdown of both *Sodh1* and *Sodh2*. Data were shown in Kaplan-Meier survival plot. One hundred flies of each genotype were tested. Significance level was established by log-rank test. NS: not significant.

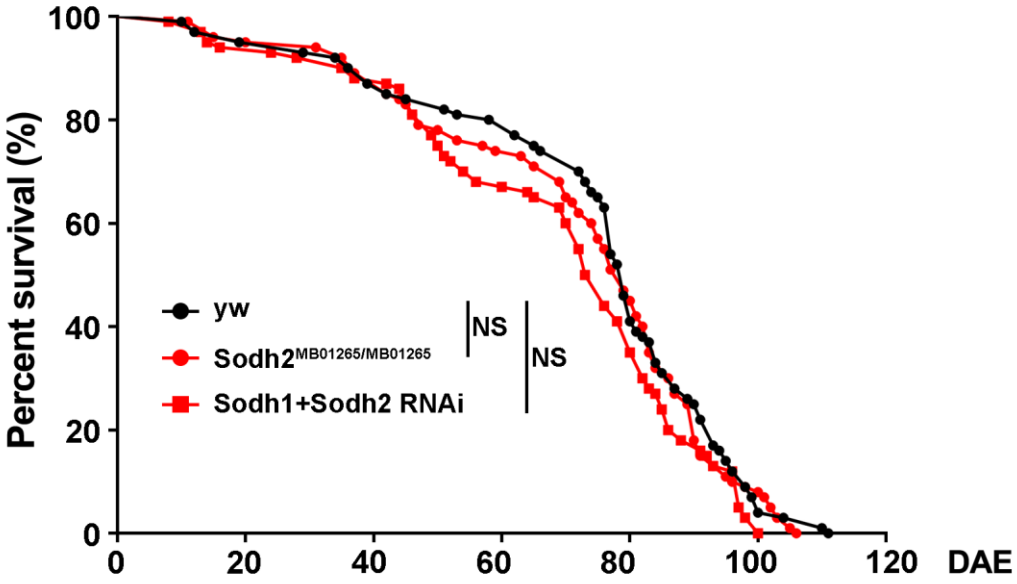

Supplementary Fig. 3. Double knockdown of *Drosophila* Sodh1 and Sodh2 causes age-dependent synaptic degeneration. A-B) Laminae of control (*GMR-GAL4* heterozygotes) or *Sodh1* and *Sodh2* double knockdown homozygous flies at 2 DAE and 10 DAE were stained with HRP (green; marks neuronal membranes) and BRP (magenta; marks synaptic active zones). Yellow arrowheads indicate vacuole-like structures in the lamina that correspond to missing terminals. The areas outlined by yellow boxes are shown at higher magnification. The intensity of BRP is indicated using a red spectrum. Dotted lines indicate the area of lamina vacuole-like structures. Scale bars: 30 μm. **C)** Quantification of the number and size of vacuole-like structures. A total of 8 laminae of each group were quantified. Data are presented as mean ± s.d.. Statistical analysis was performed using two-way ANOVA followed by post-hoc Tukey's multiple comparison test; *p<0.05, **p<0.01, ****p<0.0001.

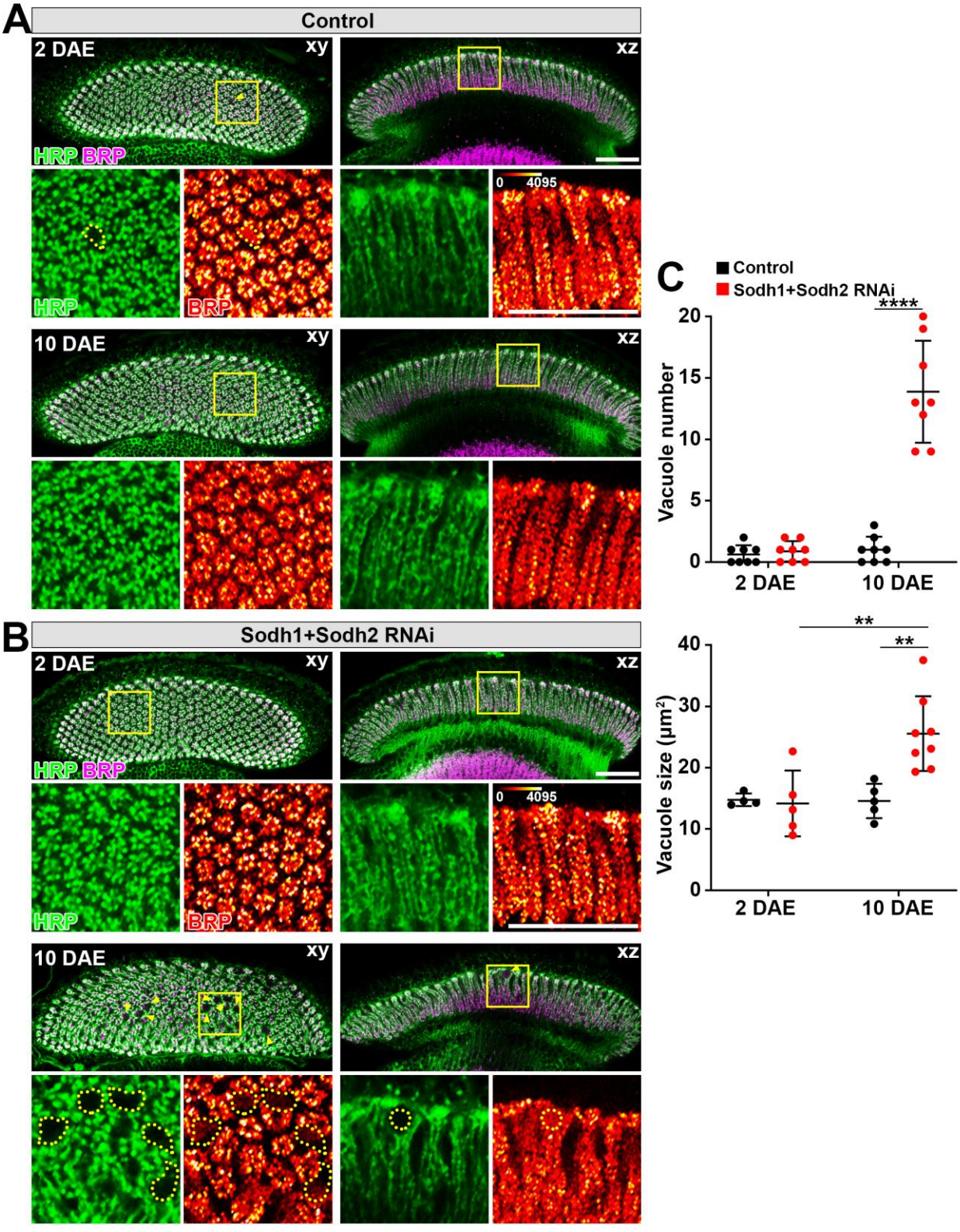
A
Control
2 DAE
xy
xz
HRP BRP
HRP
BRP
0 4095
10 DAE
B
Sodh1+Sodh2 RNAi
C
Control
Sodh1+Sodh2 RNAi
****
Vacuole number
2 DAE
10 DAE
**
**
Vacuole size (µm²)

Supplementary Fig. 4. Treatment with aldose reductase inhibitors Epalrestat and Ranirestat restore locomotor function in Sodh1 and Sodh2 double knockdown flies. Locomotor activity of control flies (yw) feeding with DMSO (black dots), or flies with neuronal specific knockdown of Sodh1 and Sodh2 feeding with DMSO (red squares), 80 μg/ml Epalrestat (blue squares), or 80 μg/ml Ranirestat (green squares). n=10 in each group. Data are presented as mean ± s.d. Statistical analysis was performed using two-way ANOVA followed by post-hoc Tukey's multiple comparison test; ***p<0.001, ****p<0.0001.

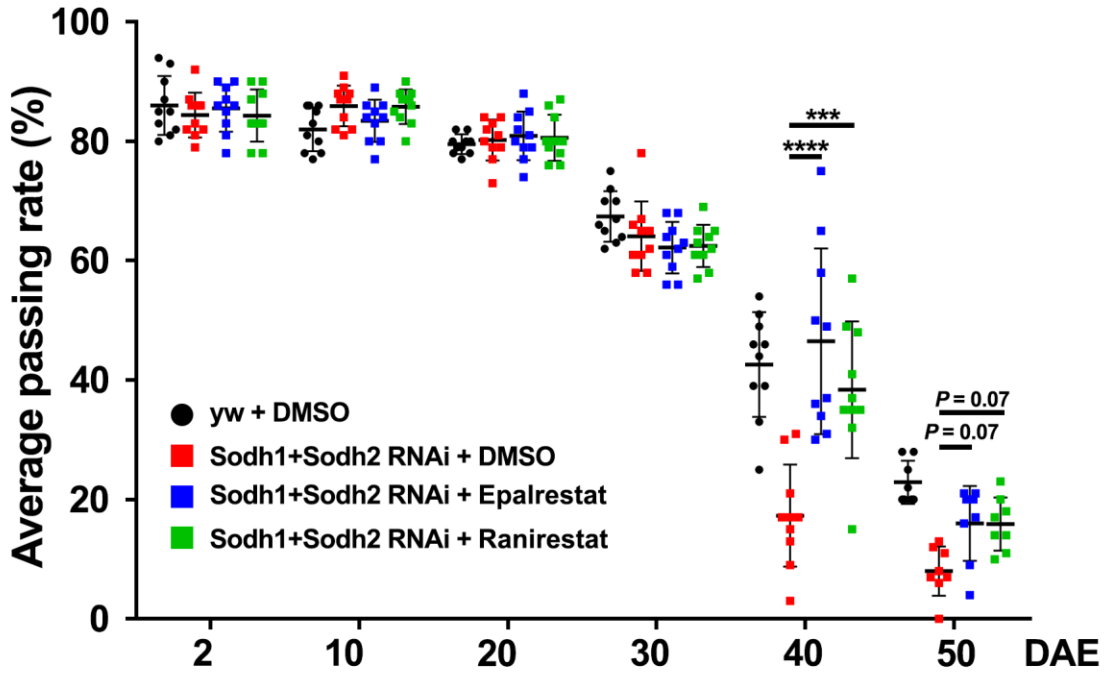

SUPPLEMENTARY TABLES

Supplementary Table 1. Primers sequences and thermocycling conditions

	Primers	Reagents	Thermocycling conditions
SORD Exon 1	Fw/sequencing: CAGGCTGGCACAAAGGAG Rv: AGTGAGGCAGGATCGGTATG	Faststart Master Mix 2X (Roche) Primers 0.5 mM genomic DNA 50 ng	95°C 4 min [95°C 30 s 65°C 30 s - Each cycle decreasing by 0.5°C 72°C 1 min] X18 cycles [95°C 30s 55°C 30s 72°C 1 min] X18 cycles 72°C 5 min
SORD Exon 2	Fw/sequencing: AGCGTGCCATTTAGCGTATC Rv: GCAGTAGACTCTGTTCTCAGCCTAAC		
SORD Exon 3	Fw ACCTTTTCTCATAAATAGATACGAATCC Rv/sequencing TCTTGTTCCCTGCTGTACCC		
SORD Exon 4	Fw and sequencing GCATGCAAGCCTTCATAACA Rv CGAGGTCATTGTTGTTATGACG		
SORD Exon 5	Fw/sequencing CGTGGCCATGTTAACTCCTT Rv GTTCCCTGAATTCCCAGTCA		
SORD Exon 6	Fw/sequencing ATGTTTAATATTTCACGAACATATTCC Rv GCTGTTTCCCAGTCAAGGAG		
SORD exon 7	Fw TGAGTCATCAGATTTCTCTTGTTTG Rv AGCCTGGGCGACTGAGTGAG Sequencing AAAAGAAAACATAGATGGCAAAAGA		
SORD exon 8	Fw/sequencing TCCCGCTCAGTTAAGTTTGG Rv GCTTCAAAATCCCCTCCTTC		
SORD exon 9	Fw/sequencing CACCTGGCTCTTTCCTCTTG Rv CCCTGAGATCCCAAGACTG		
SORD2P exon 7	Fw TGAGTCATCAGATTTCTCTTGTTTG Rv TTCAAGTACAGGCTCCACACT		

PCR: polymerase chain reaction; Fw: forward; Rv: reverse

Supplementary Table 2. Variants identified in *SORD* in patients with CMT

Chr (hg19)	cDNA	protein	GERP	Mutation Taster	Gnomad Genomes MAF
chr15:45315509	c.28C>T	p.Leu10Phe	4.54	disease causing	0
chr15:45353297	c.298C>T	p.Arg100Ter	n/a	disease causing	0.00003229
Chr15:45353315	c.316_425+165del	p.Cys106Ter	n/a	disease causing	0
chr15:45353328	c.329G>C	p.Arg110Pro	4.23	disease causing	0
chr15:45357501	c.458C>A	p.Ala153Asp	4.51	disease causing	0.0002905
chr15:45361217	c.757delG	p.Ala253GlnfsTer27	4.74	disease causing	0.003021
chr15:45353297	c.295C>T	p.Arg299Ter	n/a	disease causing	0
chr15:45365618	c.964G>A	p.Val322Ile	5.45	disease causing	0.00007325

RefSeq Transcript:NM_003104.6. MAF: minor allele frequency, n/a not available

Supplementary Table 3. Carrier frequency in gnomAD v3 database of the most common pathogenic variants associated with autosomal recessive CMT

Gene ID	Variant ID	Consequence	mutation type	Allele count	Allele number	Allele frequency
SORD	15-45069018-CG-C	p.Ala253GlnfsTer27	frameshift	623	142588	0.00437
SH3TC2	5-149026872-G-A	p.Arg954Ter	stop gained	94	143270	0.000656
GDAP1	8-74361886-C-T	p.Gln163Ter	stop gained	21	143188	0.000147
IGHMBP2	11-68939657-CAG-C	p.Arg971GlufsTer4	frameshift	25	143316	0.000174
FDG4	12-32602314-TC-T	p.Gln443ArgfsTer9	frameshift	5	143280	0.0000349

Supplementary Table 4. (separate file). Clinical features of patients with hereditary neuropathy and carrying biallelic mutations in *SORD*